CHALMERS
UNIVERSITY OF TECHNOLOGY

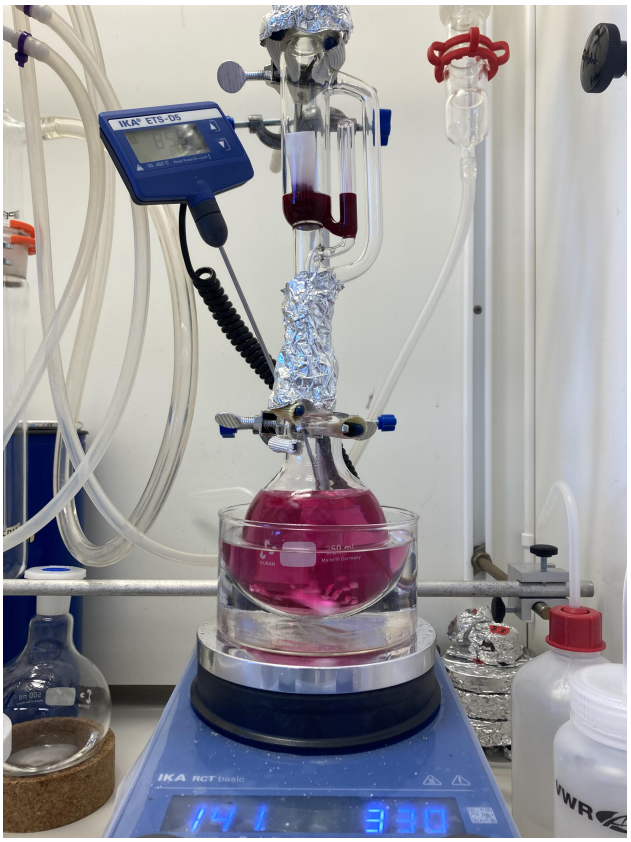

Purification of conjugated polymers

Better polymers through HPLC purification and Soxhlet extraction

Master's thesis in Materials Chemistry

JESSIKA ÖHBERG

DEPARTMENT OF CHEMISTRY AND CHEMICAL ENGINEERING
CHALMERS UNIVERSITY OF TECHNOLOGY
Gothenburg, Sweden 2024
www.chalmers.se

Master's thesis 2024

Purification of conjugated polymers

Better polymers through HPLC purification and Soxhlet extraction

JESSIKA ÖHBERG

CHALMERS
UNIVERSITY OF TECHNOLOGY

Department of Chemistry and Chemical Engineering
Division of Applied Chemistry
Alexander Giovannitti research´s group
Chalmers University of Technology
Gothenburg, Sweden 2024

Purification of conjugated polymers
Better polymers through HPLC purification and Soxhlet extraction
JESSIKA öHBERG

Supervisor: Megan Westwood, Chemistry and Chemical Engineering
Examiner: Alexander Giovannitti, Chemistry and Chemical Engineering

Master's Thesis 2024
Department of Chemistry and Chemical Engineering
Division of Applied Chemistry
Alexander Giovannitti research´s group
Chalmers University of Technology
SE-412 96 Gothenburg
Telephone +46 31 772 1000

Cover: Image of Soxhlet extraction performed on D18 with the solvent THF.

Typeset in LaTeX
Gothenburg, Sweden 2024

Purification of conjugated polymers
Better polymers through HPLC purification and Soxhlet extraction
JESSIKA ÖHBERG
Department of Chemistry and Chemical Engineering
Chalmers University of Technology

Abstract

The purification of conjugated polymers, specifically the polymer D18, was investigated using the purification methods of Soxhlet extraction and High-Performance Liquid Chromatography (HPLC). The objective was to purify D18 from residual Pd impurities remaining from synthesis and fractionate the molecular weight for lower dispersity and higher molecular weights. This is crucial for conjugated polymers like D18, as with robust and effective purification methods, they have a prominent future as materials extensively used in organic electronic devices such as solar cells. The purification process has a significant impact on the polymer's properties, influencing its electronic and optical performance which highlights the importance of standardized purification and reproducible results. The study demonstrates that while Soxhlet extraction was effective in removing low molecular weight fractions, HPLC proves to be superior in narrowing down the dispersity and reducing palladium (Pd) content for the polymer D18. The work also investigates the use of TOF-SIMS for measuring Pd content before and after purification by developing a calibration curve. Two palladium complexes, $Pd(PPh_3)_4$ and $Pd_2(dba)_3$ chloroform adduct, were along with the polymer P3HT used to create calibration curves, with $Pd_2(dba)_3$ showing better performance due to its solubility and stability. Challenges included potential contamination, suggesting the need for stricter environment protocols for sample handling. Calculating the Pd content from the calibration curves underscored the importance of a robust normalization technique to obtain absolute quantification. This research provides insights into purification methods that can enhance the performance of conjugated polymers in organic electronic applications and demonstrates the use of TOF-SIMS as an evaluation method of metal impurities.

Keywords: Conjugated polymers, Purification, Soxhlet extraction, HPLC, TOF-SIMS.

Acknowledgements

I would like to extend my deepest gratitude to my examiner, Alexander Giovannitti, whose investment in my work has been inspiring. His guidance, thoughtful feedback, and care greatly lifted my research experience. I am very thankful for his dedication, support, and for leading and bringing together a research group that has been an endless source of support, motivation, and great comradeship. I am very grateful for the valuable knowledge and experience I gained.

I am highly thankful to Per Malmberg, docent in Chemistry, Biochemistry, and Chemical Engineering for his dedication and time spent developing a method with TOF-SIMS. Without his expertise, support, and effort this work would not have been possible.

I am also highly grateful to my supervisor, Megan Westwood, who has shown me extraordinary support. Her boundless guidance, help, enthusiasm, feedback, and care for my work were invaluable. Megan's commitment to my success has been evident and I have learned so much under her supervision. Her frequent check-ins, concern, and knowledge have inspired me greatly and made this journey highly fulfilling.

I would also like to give a huge thanks to Jessica Itxel Vasquez Matias, whose expertise and support made a significant impact on my research. Her skills in teaching and guidance have taught me so much and have been immensely important for my work. I am very grateful for all the help I received as well as her unwavering positivity that always managed to brighten my days.

I am grateful to the members of my group, Aqila Naseri, Albin Petrén, and Jessica Orrego Hernandez, whose companionship and assistance have been a constant source of motivation and joy. Their presence made my work more enjoyable and our friendship was a highlight of this experience.

Lastly, I would like to express my appreciation to everyone on floor 8. The daily kindness, friendship, and support made each day something to look forward to. Their help, shared laughs, and company turned this journey into a memorable and joyful experience.

To all of you, thank you for making this work a remarkable experience, for teaching me so much, and for all the support and friendship.

Jessika Öhberg, Gothenburg, June 2024

List of Acronyms

Below is the list of acronyms that have been used throughout this thesis listed in alphabetical order:

BDT	Benzodithiophene
CPs	Conjugated Polymers
DTBT	Dithienobenzothiadiazole
GPC	Gel Permeation Chromatography
HPLC	High-Performance Liquid Chromatography
M_n	Number Average Molecular Weight
M_w	Weight Average Molecular Weight
M_W	Molecular Weight
OECT	Organic Electrochemical Transistor
OFET	Organic Field-Effect Transistor
OPV	Organic Photovoltaic
ORR	Oxygen Reduction Reaction
P3HT	Poly(3-hexylthiophene)
Pd	Palladium
PCE	Power Conversion Efficiency
PDI	Polydispersity Index
TEA	Triethylamine
THF	Tetrahydrofuran
TOF-SIMS	Time-of-Flight Secondary Ion Mass Spectrometry

Contents

List of Acronyms viii

List of Figures xii

List of Tables xiv

1 Introduction 1
1.1 Aim . . . 2

2 Theory 3
2.1 CPs . . . 3
2.1.1 Polymer D18 . . . 3
2.1.2 Purity and M_W effects on electronic properties . . . 4
2.2 Purification of CPs . . . 5
2.2.1 Soxhlet extraction . . . 5
2.2.2 Preparative recycling HPLC . . . 6
2.2.3 Analytical gel permeation chromatography (GPC) . . . 7
2.3 TOF-SIMS . . . 7

3 Methods 9
3.1 Method development for monitoring metal traces in polymers using TOF-SIMS . . . 9
3.1.1 Development of the calibration curve . . . 9
3.1.2 Pd content determination . . . 10
3.2 Polymer purification . . . 10
3.2.1 Soxhlet extraction . . . 10
3.2.2 HPLC . . . 11
3.3 Measurement of M_W and Đ with GPC . . . 11

4 Results 13
4.1 Method development of TOF-SIMS . . . 13
4.1.1 Calibration curve using $Pd(PPh_3)_4$ complex . . . 13
4.1.2 Calibration curve using $Pd_2(dba)_3 \cdot CHCl_3$ complex . . . 15
4.2 Purificiation of D18 . . . 17
4.2.1 Soxhlet extraction of D18 . . . 17
4.2.2 HPLC purification of D18 . . . 19
4.3 TOF-SIMS data analysis of polymer D18 . . . 22

4.3.1 Nonnormalized data measurement 22
4.3.2 Normalized data measurement 24

5 Discussion **28**

Bibliography **32**

A Appendix 1 **I**

List of Figures

2.1 Chemical structure of D18. 4
2.2 Schematic of a Soxhlet extractor[28]. 6

4.1 Calibration curve created from polymer samples with 0, 1, 10 100, 1000, 10,000 ppm Pd from $Pd(PPh_3)_4$. The average peak area and concentration of each sample are plotted on the y-axis and x-axis, respectively. Standard deviation can be observed in the bars for each Pd point. 14
4.2 Calibration curve created from polymer samples with 0, 1, 10 100, 1000, 10,000 ppm Pd from $Pd(PPh_3)_4$. The average peak area and concentration of each sample normalized to total ion intensity count are plotted on the y-axis and x-axis, respectively. Standard deviation can be observed in the bars for each Pd point 15
4.3 Calibration curve created from polymer samples with 0, 1, 10 100, 1000, 10,000 ppm Pd from $Pd_2(dba)_3 \cdot CHCl_3$ complex. The average peak area and concentration of each sample are plotted on the y-axis and x-axis, respectively. Standard deviation can be observed in the bars for each Pd point. 16
4.4 Calibration curve created from polymer samples with 0, 1, 10 100, 1000 ppm Pd from $Pd_2(dba)_3 \cdot CHCl_3$ complex. The average peak area and concentration of each sample are plotted on the y-axis and x-axis, respectively. Standard deviation can be observed in the bars for each Pd point. 17
4.5 Chromatogram of GPC analysis for fractions from Soxhlet extraction with the solvents THF and $CHCl_3$, respectively. 19
4.6 UV-vis spectra from the purification of D18 illustrating the absorbance of compounds detected at 350, 400, 550, and 700 nm and the time of the manual separation. 20
4.7 Chromatogram of GPC analysis for fractions from HPLC purification. 22
4.8 Pd content from in-depth profiling of neat D18 and D18 samples collected from HPLC purification and Soxhlet extraction calculated from the regression model. The measurement of D18 samples is nonnormalized and standard deviation is seen as the bars for each sample point. 23

4.9 Calibration curve normalized to an alkane fragment created from polymer samples with 0, 1, 10 100, 1000 ppm Pd from $Pd_2(dba)_3 \cdot CHCl_3$ complex. The average peak area and concentration of each sample are plotted on the y-axis and x-axis, respectively. Standard deviation can be observed in the bars for each Pd point. 25
4.10 Pd content from in-depth profiling of neat D18 and D18 samples collected from HPLC purification and Soxhlet extraction calculated from the regression model. The measurement of D18 samples is normalized to an alkane fragment and the standard deviation is seen as the bars for each sample point. 26

List of Tables

4.1 The M_n, M_w and Đ measured with GPC for fractions from Soxhlet extraction with the solvents THF and $CHCl_3$, respectively. 18
4.2 Polymer mass collected from each D18 fraction purified with HPLC. . 20
4.3 The M_n, M_w and Đ measured with GPC for fractions from the collected fractions of HPLC purification. 21
4.4 The average amount of Pd^+, $^{108}Pd^+$, and $^{105}Pd^+$ in ppm calculated for each D18 sample from the in-depth profiling with TOF-SIMS and nonnormalized. 24
4.5 The amount of Pd^+, $^{108}Pd^+$ and $^{105}Pd^+$ in ppm calculated for each D18 sample from the in-depth profiling with TOF-SIMS and normalized to alkane fragment. 27

A.1 Amounts of used $Pd(PPh_3)_4$ and chlorobenzene for serial dilution to create concentrations of 1, 10, 100, 1000, 10,000 ppm in polymer solution. I
A.2 Amounts of used $Pd_2(dba)_3 \cdot CHCl_3$ and chlorobenzene for serial dilution to create concentrations of 1, 10, 100, 1000, 10,000 ppm in polymer solution. I

1

Introduction

Redox-active polymers are a promising class of materials for the development of novel electronic applications[1]. Specifically, conjugated polymers (CPs) that possess charge transport properties have been studied and used in several application areas such as organic photovoltaic (OPV) devices[2][3][4], and organic field-effect transistors (OFET)[5]. If these materials are designed properly they have the potential to replace inorganic materials with several benefits such as less toxicity, less hazardous waste, good recycling possibilities, and reduced unsustainable extraction of raw materials[6][7]. CPs can be produced at a large scale and their versatile synthesis routes offer easy and convenient design with great tunability, functionalization, and optimization opportunities[6].

The structure of CPs in solid state largely influences their optoelectronic properties due to their semi-crystalline nature. The solid-state structure in turn relies on the molecular weight (M_W) and dispersity (Đ) as well as any potential impurities. Although some purification techniques are carried out after synthesis, the metal catalyst can degrade and bind to the polymer backbone or side chains so that it remains in the final polymer.[3]. It has been found in studies for OPV devices that the presence of palladium (Pd) leads to lower photocurrent by the formed aggregates of Pd acting as short circuits that create leakage pathways[3]. The power conversion efficiency (PCE) of a solar cell has been observed to decrease when Pd or Ni remains in the polymer after synthesis.[3][2]. Additionally, for some polymers, Pd impurities led to the formation of traps that aid charge carrier recombination[3]. For other devices such as OFETs and organic electrochemical transistors (OECTs), the presence of Pd and Ni resulted in reduced charge carrier mobility[8][9] and catalyze undesired reactions such as oxygen reduction reaction (ORR) which may form hydrogen peroxide (H_2O_2)[8].

The M_W and Đ of CPs has also been found to impact the performance of organic electronic devices based on them[10][11][12]. The charge transport mechanisms in CPs depend upon the intermolecular and intramolecular movement of charge carriers through the material. Where there are crystallites there is the ability to have hopping of holes or electrons between adjacent chains[13]. Intramolecular charge transport occurs along the conjugated portion (backbone) of the polymer where it is planar. The longer this conjugation length is the better it therefore is to get charge traveling through the material[13]. As a result, in electronic applications, it is important to remove monomers and oligomers. Several studies have approved this in which higher M_W has been linked to increased charge transport properties for an

OECT device[11]. Additionally, the electrochemical stability has been reported to be enhanced by a higher M_W for a polymer studied for its usage in optoelectronic devices[12][10].

By carrying out the purification of CPs to both fractionate the M_W and therefore reduce Đ and remove impurities from synthesis, the performance of devices made from OSCs can be improved. In particular, the removal of residual metals from CPs is important as their presence can cause misinterpretation of results in applications such as electrocatalysis where Pd can catalyze the ORR to form water. It is therefore important to establish standardized protocols to realize more effectively purified CPs with high reproducibility of organic electronic materials. Furthermore, batch-to-batch variations will be limited to improve standardized studies in the field of OSC research. This would have a profound impact on the future materials used for electronic devices and offer several social, economic, and environmental benefits compared to inorganic materials such as cost-effectiveness regarding the abundance of raw material, and resistance towards corrosion. The environmental benefits include the use of earth-abundant materials that do not require extensive mining and the potential of recycling of materials.

1.1 Aim

This study aims to develop a method to measure Pd content in the CP D18. It is done by creating a calibration curve using the CP P3HT through the time-of-flight secondary ion mass spectrometry (TOF-SIMS) technique. Furthermore, conventional purification methods are investigated and compared, specifically Soxhlet extraction and preparative high-performance liquid chromatography (HPLC). The developed TOF-SIMS method is then used to measure the Pd content of purified D18 samples.

2

Theory

2.1 CPs

CPs are organic molecules characterized by alternating single and double bonds over their backbone chain[14]. This results in delocalized π-electrons along the polymer chain and gives electronic and optical properties such as the capability of carrying and storing charge[14][15][16]. Hence, CPs are attractive for several electronic applications[14]. The delocalizations of π bonds result in bonding π-bands and antibonding π bands[17]. The energy gap between these bands affects the electronic and optical properties of the CP. This energy gap in turn depends on the structure of the polymer, specifically the backbone and substituents[17]. Furthermore, doping is commonly performed with electron donors or acceptors to introduce charge carriers[17]. Physical properties such as M_W, purity, and crystallinity also affect the conductivity and therefore the resulting performance of an organic electronic device[17][4].

2.1.1 Polymer D18

The polymer D18 has gained significant attention in the field of organic electronics, particularly in OPVs[18][19]. Its chemical structure is seen in Figure 2.1 and consists of a backbone that has alternating electron-donating benzodithiophene(BDT) and electron-accepting fused-ring dithienobenzothiadiazole (DTBT) units[20]. This donor-acceptor structure of D18 contributes to its unique electronic and optical properties[19]. It promotes efficient charge transport and light absorption which makes it a promising material for organic solar cells[21][19]. A recent study of a polymer-based bulk heterojunction (BHJ) solar cell achieved a PCE of over 18% using D18 as a donor polymer and Y6 as a small molecule acceptor[22]. The study shows the prospect of D18 being used on a large scale for organic solar cells and hence, in commercial applications.

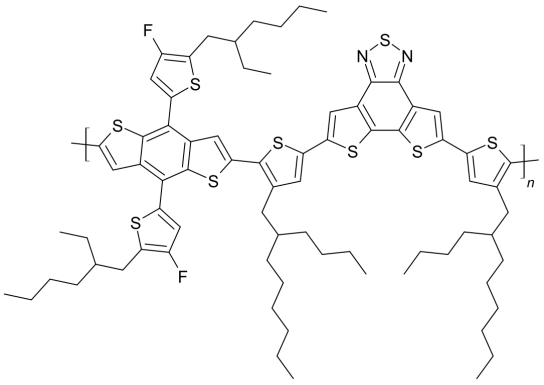

Figure 2.1: Chemical structure of D18.

The structure of D18 with its alternating electron donor and acceptor units results in a narrower energy band gap compared to other CPs which improves its ability to transport charge carriers and in addition, absorb visible light[20]. D18 absorbs strongly in the visible light spectrum with its intramolecular charge transfer (ICT) band at around 500-700 nm which is essential for reaching high PCE in organic solar cells[23]. D18 is a p-type semiconductor and the conductivity among others also depends on several physical factors such as M_W, crystallinity, morphology [20][21][24][23], and the purity of the polymer. D18 can be dissolved by the chlorinated solvents chloroform, chlorobenzene, and dichlorobenzene[20]. However, higher M_W show poorer solubility in solvents which limits their utilization in organic solar cells[20]. Higher M_W are favorable for an ordered and crystalline structure which enhances charge transport properties[24].

2.1.2 Purity and M_W effects on electronic properties

The electronic and optical properties of CPs are significantly influenced by the chemical composition and structural integrity of the microstructure in films[13][3]. The purity of CPs after synthesis is therefore a central aspect of the performance in constructed organic electronic devices. D18 is synthesized through Stille coupling using a Pd complex as a catalyst which can remain in the final polymer, thus limiting its efficient usage in electronic applications[22][18]. Residual Pd in the polymer matrix can increase charge recombination and act as short circuits thus reducing charge carriers and altering its pathways.[3]. This is a crucial issue for D18 used in organic solar cells that rely on high PCE.

The M_W and Đ have also been found to impact the performance of OPVs based on CPs[10][12]. Previous studies on CPs for solar cell applications have found that a higher M_W led to increased PCE, however, up to a certain critical point after which it started to decrease[10]. The increased M_W increases the conjugation length of polymer chains which improves charge carrier mobility[10][11][12]. In addition, higher M_W tend to decrease solubility and form aggregates which affect its processability and morphology[10]. Regulation of the M_W is therefore also of importance to realize the large-scale production and commercialization of organic solar cells. Reproducible batches with the same degree of purity, M_W, and Đ are essential for

creating organic solar cells with reproducible performance.

2.2 Purification of CPs

The purification of CPs is essential for eliminating Pd impurities and purifying the M_W. Several methods have been used to remove Pd with varying degrees of success including metal scavenging and Soxhlet extraction[4][25]. Soxhlet extraction can, in addition, purify the M_W of CPs but its effect on D18 has limited studies. Another method to separate a CP into M_W fractions is size exclusion chromatography which has also been found to remove Pd impurities in CPs[25][8].

2.2.1 Soxhlet extraction

Soxhlet extraction is a solid-liquid separation technique commonly used for compounds with a low degree of solubility in a solvent in which impurities are insoluble[26]. It consists of a Soxhlet extractor in which a porous thimble is placed with the crude polymer sample. A chosen solvent is heated to reflux and condensed into the Soxhlet thimble[26]. The schematic of a Soxhlet extractor is shown in Figure 2.2 in which the sample is placed within the extraction chamber and the siphon arm empties the condensed solvent into the flask when the chamber is full. The efficiency of the separation is dependent on the ability of the solvent to dissolve and extract impurities[26]. Several solvents are typically used such as the anti-solvents methanol, acetone, and hexane to remove impurities and low M_W material. Finally, solvents such as chloroform and chlorobenzene are used to extract the final polymer. The washing of the polymer is done for 24 hours[27]. Soxhlet extraction is also used to remove residual monomers and low M_W chains to narrow the Đ[27]. However, its success in removing most commonly Pd metal impurities has been reported to be poor in literature, removing only minor amounts[8][25][4].

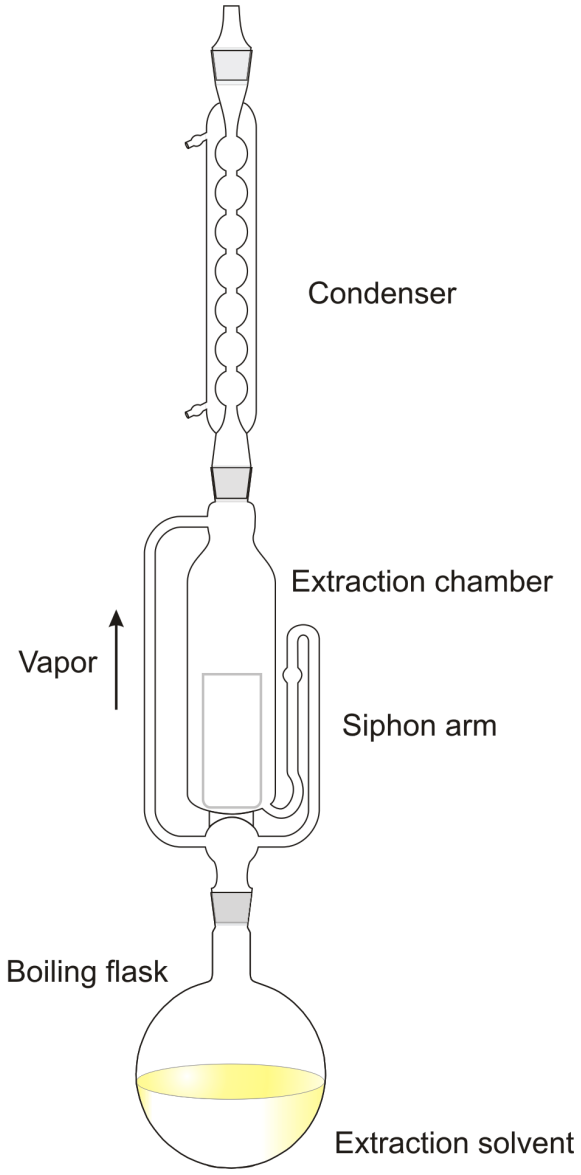

Figure 2.2: Schematic of a Soxhlet extractor[28].

2.2.2 Preparative recycling HPLC

Preparative recycling HPLC is a liquid chromatography technique in which the separation of analytes is based on size exclusion[29]. In recycling HPLC, the eluent can be redirected back into the column for additional separations which increases the effective column length and allows for separation of closely eluting compounds[30]. Size-exclusion chromatography (SEC) functions by separating based on hydrodynamic volume in which smaller molecules diffuse into the porous gel material in the column while larger ones are unaffected, hence molecules that are larger than the pore size elute first[30][29]. The technique can be used to sort polymer chains by chain length, narrow distributions, and purify CPs[8]. Metal impurities have a major difference in molecular mass compared with the polymer chains of interest, thus SEC is a good technique to remove it from the polymer. Although it has been

shown that the Pd content in CPs can be reduced using HPLC, further development of this technique could allow high reproducibility between polymer batches[8]. A study on the purification of two CPs found that purification by HPLC decreased the Pd concentration ranging from 54 and 97% compared to unpurified fractions[8]. The resulting Pd content was as low as 39 and 73 ppm which was described as a validation of using for purification[8]. In another study, the F8BT polymer synthesized by Suzuki polymerization using a Pd catalyst was purified by HPLC which resulted in a reduction from 1170 to 195 ppm in Pd content[25].

2.2.3 Analytical gel permeation chromatography (GPC)

Analytical GPC is a size-exclusion technique used to measure the M_w and Đ of polymers[29]. It operates on the same principle as preparative HPLC with porous material in a column that the samples flow through in a solvent. Smaller molecules penetrate deeper into the pores and experience a longer path, while larger molecules pass through and elute more quickly[29]. The result is a UV-vis chromatogram where the elution volume correlates with the size of the polymer molecules[29]. A calibration curve often made with polystyrene standards is then used to determine M_W and Đ[31]. A polymer does not have a single value for its molecular weight due to different chains with varying lengths and different numbers of side branches[32]. It is therefore measured as a distribution of chain lengths and the number average molecular weight (M_n), weight average molecular weight (M_w), and Đ[29] are obtained from the analytical GPC. M_n is defined as the total weight of all polymer molecules in a sample divided by the total number of molecules. This measure gives equal weight to each molecule regardless of its size[32]. M_w in turn accounts for the size of the molecules which gives more weight to larger sizes. It reflects the polymer's contribution to its overall weight, thus it is always a larger value than M_n[32]. The Đ is the ratio of M_w to M_n and provides a measure of the distribution of molecular weight within a given polymer sample[32]. It has values of 1 or greater than that, where if it is equal to 1, it is a monodisperse sample with molecules of the same weight. Hence, a larger value indicates a broader spread of molecular weights[32].

2.3 TOF-SIMS

Time-of-Flight Secondary Ion Mass Spectrometry (TOF-SIMS) is an analytical technique used to analyze the composition of a sample surface[33][34]. It functions by bombarding the sample with a primary ion beam and the ejected secondary ions from the sample are then detected and analyzed. This technique results in detailed information about elements, isotopes, and molecular composition on the surface of a sample. The source of the primary beam can be a variety of ions such as Ar+ and oxygen species which is then focused on the sample[33][34]. Sputtering of the source can also be used besides measuring the surface to obtain a depth profile of the sample in which the beam digs through the thickness of the sample. The emitted secondary electrons from the sample are then accelerated through the times of the flight tube[33][34]. The time it takes for an ion to travel to the detector is proportional to its mass-to-charge ratio(m/z) which is then converted into a mass

spectrum. This mass spectrum shows the m/z of each detected ion. TOF-SIMS is a highly sensitive technique with the capability to detect any isotopes and traces of elements[33][34].

A sample is often measured at multiple different areas with TOF-SIMS and the results can also be in the form of the average intensity of signals or ion counts across a scanned area. Thus, with a calibration curve with known concentrations, it is possible to quantify the amount of a certain element in the sample besides obtaining a mass spectrum.

3

Methods

3.1 Method development for monitoring metal traces in polymers using TOF-SIMS

In the following chapter, the development of a calibration curve to utilize TOF-SIMS for measuring polymer samples is discussed. The subsequent use of the calibration curve for determining Pd content in D18 samples purified with the methods, Soxhlet extraction and HPLC, along with measurement of M_W and Đ, is explained.

3.1.1 Development of the calibration curve

To investigate Pd concentration in a range of purified CP samples, a calibration curve was developed for TOF-SIMS in which known palladium content in conjugated polymer samples was added and then measured. This was performed using a CP that was synthesized without Pd and known quantities of a Pd catalyst were added. Two calibration curves were created using thin films of P3HT and two different Pd complexes. For the first calibration curve, the complex tetrakis(triphenylphosphine)palladium(0) ($Pd(PPh_3)_4$) was used, and for the second dipalladium-tris(dibenzylideneacetone) chloroform adduct, $Pd_2(dba)_3 \cdot CHCl_3$. To prepare films containing each of the complexes, a series of dilutions was done of a Pd stock solution to create a Pd concentration of 1, 10, 100, 1000, and 10,000 ppm in polymer solution. Chlorobenzene was used as a solvent in 5 different vials in which the Pd complexes were added into the first vial giving the Pd concentration of 10,000 ppm in polymer solution. The amounts used and the subsequent serial dilution can be seen in Appendix 1.

For preparing films, a solution of P3HT in chlorobenzene (10 mg/ml) and 25 μl of catalyst solution (Appendix 1) was added. Thin films were prepared using silicon wafers that were cut into 1x1 cm pieces. The cut films were then washed by placing them in holders in a beaker that was filled with different solvents and sonicated for 15 minutes, respectively. Ultrapure water with normal dish soap was used first which was then followed by ultrapure water, acetone, and isopropanol. The films were then dried with nitrogen gas by holding them with a tweezer to avoid damage and contamination and placed in a petri dish. When using the $Pd(PPh_3)_4$ complex, around 100 μl of the polymer and Pd solution was spin-coated onto the films. For each palladium concentration under study, 2 films were prepared for TOF-SIMS measurement which consisted of 100 μl of the neat polymer solution and the polymer solution with 1, 10, 100, 1000, and 10,000 Pd concentrations, respectively. After

spin-coating, the samples were stored under nitrogen until measurement.

When developing the second calibration curve using the $Pd_2(dba)_3 \cdot CHCl_3$ complex, the polymer solutions were drop-casted onto the films. The fume hood was cleaned to reduce contamination when thin films were placed on it for drop-casting. Around 3 μl was used for each sample solution and glass dishes were placed over the films after coating to slow down evaporation for an even surface. The dishes were periodically opened until the solution had dried. This was followed by drying the samples overnight in a vacuum oven using a static vacuum until measurement.

The subsequent measuring of the Pd content on the thin film samples was carried out TOF-SIMS utilizing both surface analysis and in-depth profiling. The measurements were done on the instrument IONTOF 5 using the software Surface Lab v7. For the calibration curve using the $Pd(PPh_3)_4$ complex, argon was used as a source, and for the $Pd_2(dba)_3 \cdot CHCl_3$ complex both argon and oxygen were used. The measurements were done automatically overnight and 4 different areas of each sample were measured. For analysis of the data, the average peak area and intensity were collected for the Pd^+ content and the two isotopes $105Pd^+$, and $108Pd^+$ to enable the creation of a calibration curve. This was done by taking the average peak area of a chosen isotope signal over the 4 sample areas and plotting it against the known Pd concentration in ppm, including the standard deviations in the plot.

3.1.2 Pd content determination

To test Pd content in polymer samples, thin films were prepared for TOF-SIMS measurements. The films were prepared and cleaned in the same procedure that was done for the calibration curve described in section 3.1.1. The samples consisted of the D18 fractions that were collected from HPLC and Soxhlet purifications and compared against the unpurified D18 sample. Each sample was dissolved in chloroform to a concentration of 10 mg/ml. Drop-casting was used to coat each thin film with a sample solution. Around 5 μl of each solution was dropped onto the thin films and glass dishes were used to cover the films which were periodically opened. After drying, the coated films were placed in a vacuum oven with a static vacuum overnight until measurement.

The measurement of Pd content with TOF-SIMS was done on IONTOF 5 using the software Surface Lab v7 utilizing argon as a source for surface analysis and in-depth profiling. 3 different areas were measured for each sample which consisted of 2 films. The analysis was performed automatically overnight and the average peak area and intensity were collected for the Pd^+ content, and the two isotopes $105Pd^+$, and $108Pd^+$ for subsequent data interpretation.

3.2 Polymer purification

3.2.1 Soxhlet extraction

Soxhlet extraction was performed for D18 using the following order of solvents methanol, acetone, hexane, THF, and chloroform. 100 mg of neat D18 was added

to a cellulose thimble within a Soxhlet condenser. 250 ml round bottom flask was filled up to two-thirds of the bottle for each solvent and the flask was placed in an oil bath. A hotplate was used for heating the oil bath and an air condenser connected to nitrogen flow was used for condensation. Solvents were stirred and condensed into the thimble to wash out impurities and low M_W fractions. The extraction was done for 24 hours with methanol and acetone and for hexane, Tetrahydrofuran (THF), and chloroform until no color could be observed in the Soxhlet condenser. Methanol is used to remove residual catalysts and other byproducts. Extraction using acetone is followed which removes monomers and oligomers. Hexane and THF extended this by removing low molecular weights. The last step is the extraction of D18 using chloroform. Between the use of each solvent, the remaining solvent was removed and collected to not blend the different fractions. Each solvent fraction was then dried using a rotary evaporator which for the THF and chloroform fraction was followed by dissolution in chloroform and precipitation with methanol. Vacuum filtration was done over a PTFE membrane (pore size 0,45 μm) to collect the dry mass which was then dried in a vacuum oven at 40 °C.

3.2.2 HPLC

Schlenkline technique was used to prepare an air and moisture-free environment when preparing the neat polymer solution. The Schlenk flask was heated and then put under a vacuum which was followed by nitrogen flow which was repeated 3 times to dry the glassware. To prepare the HPLC mobile phase, 12,5 mL of triethylamine (TEA) was added to 2,5 L of HPLC grade chloroform to give a 0,5% concentration of TEA. Neat D18 was dissolved in chloroform HPLC grade to give a concentration of 10 mg/ml. The polymer solution was subsequently stirred for an hour at 500 rpm. Afterward, the solution was filtered through a 0,45 μm PTFE syringe filter. HPLC separation was performed with the instrument LaboACE LC-7080 Plus from Japan Analytical Industry Co.,Ltd using a JAIGEL-4HR column. According to the literature, D18 absorbs strongly at 550 nm so this wavelength was followed through the HPLC separation with ultraviolet (UV) detection using the chromatography software JAI scan[23]. The separation was performed with two recyclings to extend the effective column length for improved separation. A high, medium, and two low M_W fractions were then collected by manual operation of the fraction collector into round-bottomed flasks. After the HPLC separation, each fraction was evaporated using a rotary evaporator. To obtain dry polymer samples, the fractions were then isolated by complete dissolution in chloroform and subsequent precipitation in methanol followed by vacuum filtration. The fractions were collected onto filtration paper and placed in amber vials that were put under a vacuum for drying. After complete drying, the fractions were weighed.

3.3 Measurement of M_W and Đ with GPC

Each sample was diluted with chloroform HPLC grade to give a concentration of 1 mg/ml. This was followed by filtration using a 0,45 μm PTFE syringe filter into GPC vials. Analytical size exclusion chromatography was carried out using an

Agilent 1260 Infinity II instrument equipped with 3x SDV columns supplied by PSS connected in series. Calibration was carried out using narrow polystyrene standards between 500-2.5 MDa. Analysis was carried out using refractive index (RI) detection with chloroform as the mobile phase at 35 °C.

4

Results

4.1 Method development of TOF-SIMS

In the following chapter, the development of a TOF-SIMS calibration curve is discussed. Subsequently, various polymer purification methods are used and the resulting Pd content is analyzed using the developed analytical technique.

4.1.1 Calibration curve using $Pd(PPh_3)_4$ complex

The resulting thin films that were made from P3HT and Pd solutions utilizing spin-coating had a thin and slightly uneven coating of the solutions. After sputtering the sample using argon as a source, the intensity of a given ion fragment can be detected. To analyze the relative amount of each mass fragment, the average area of the peak is taken over the 6 sample areas. In Figures 4.1 and 4.2 the concentrations can be seen on the x-axis and the average peak area on the y-axis. Figure 4.1 illustrates the average peak area, before normalization. Pd^+ and the two isotopes $^{108}Pd^+$ and $^{105}Pd^+$ were detected in the samples which are stable and naturally occurring isotopes. The presence of Pd was observed in the neat P3HT sample which could be caused by contamination. Although thorough care was taken during sample preparation, atmospheric or cross-contamination may have occurred during setting up the measurements. For the neat P3HT and lower Pd concentrations of 1 and 10 ppm, a significant standard deviation is seen in Figure 4.1 which means that the Pd concentration varied to a large extent for the different measured areas. Furthermore, no apparent pattern in standard deviation for Pd^+ and the isotopes was observed. Although the measured concentration of Pd in the 10 ppm sample had a higher average peak area than the 1 ppm sample, the overlap of the standard deviations means that there is no significant difference between the two values. Following the 10 ppm Pd concentration is 100 ppm which shows a decrease in measured Pd, however, the standard deviation is smaller for this sample. The 1000 and 10,000 ppm samples proved to be more successful and showed increased Pd content and reduced standard deviation for the 1000 ppm sample. This indicates that at a Pd content under 100 ppm, there's a large amount of sampling error meaning that the measured peak areas are not significantly different between the samples 0, 1, and 10 ppm. This is also the case for the 100 and 1000 ppm samples even though the standard deviation is lower and it is only the 10,000 ppm sample that is significantly different.

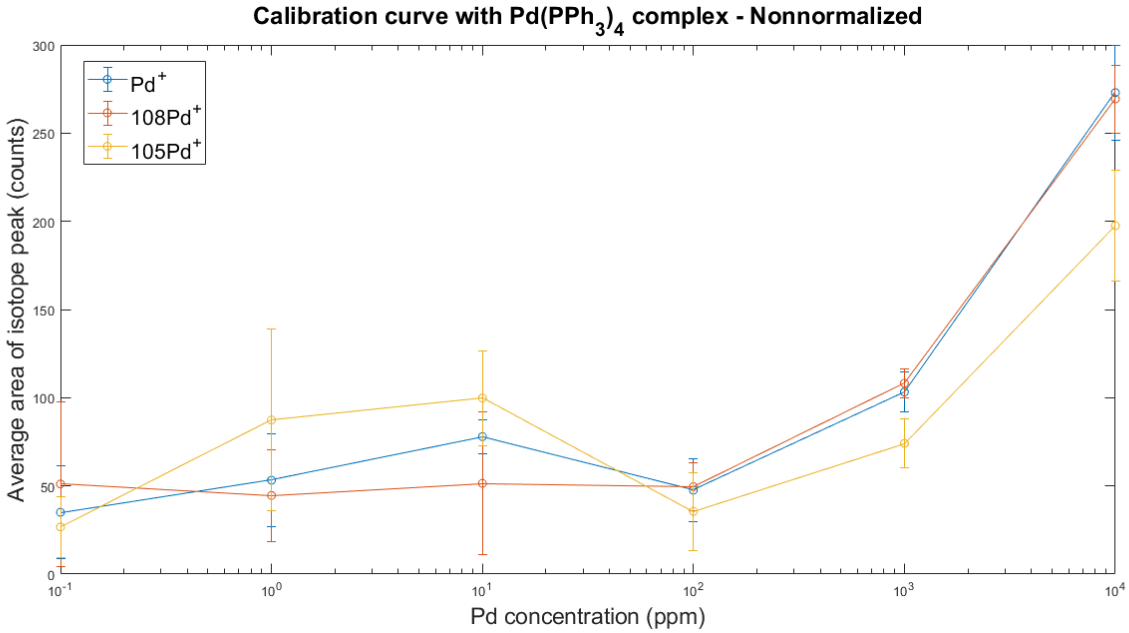

Figure 4.1: Calibration curve created from polymer samples with 0, 1, 10 100, 1000, 10,000 ppm Pd from $Pd(PPh_3)_4$. The average peak area and concentration of each sample are plotted on the y-axis and x-axis, respectively. Standard deviation can be observed in the bars for each Pd point.

In Figure 4.2, the same samples were measured, however, the values were normalized to total ion intensity count. This was done to account for variations in experimental conditions such as ionization efficiency and therefore provide a better linear fit. The presence of Pd was detected for the neat P3HT and showed a major standard deviation for the two Pd isotopes. A slight decrease in standard deviation is observed for 1 and 10 ppm Pd concentration samples, whereas, a major decrease is seen for 100, 1000, and 10,000 Pd concentration samples. The Pd^+ is observed to decrease the most for all samples. Since Pd^+ is an aggregated signal of the total Pd content from all isotopes it could be less susceptible to variations between samples due to a higher total count. Small variations of the isotope's natural abundance between samples or differences in ionization energy can be more noticeable for specific isotope signals compared to the overall Pd^+ signal. Normalizing the data seems to have a better linear fit since it accounts for variations in experimental conditions such as ionization efficiency. However, the expected linear trend in Pd content was not observed. The measured Pd content appeared overestimated for the low concentrations of 0-100 ppm with a significant overlap in the standard deviation values meaning that the differences in the samples were not significant.

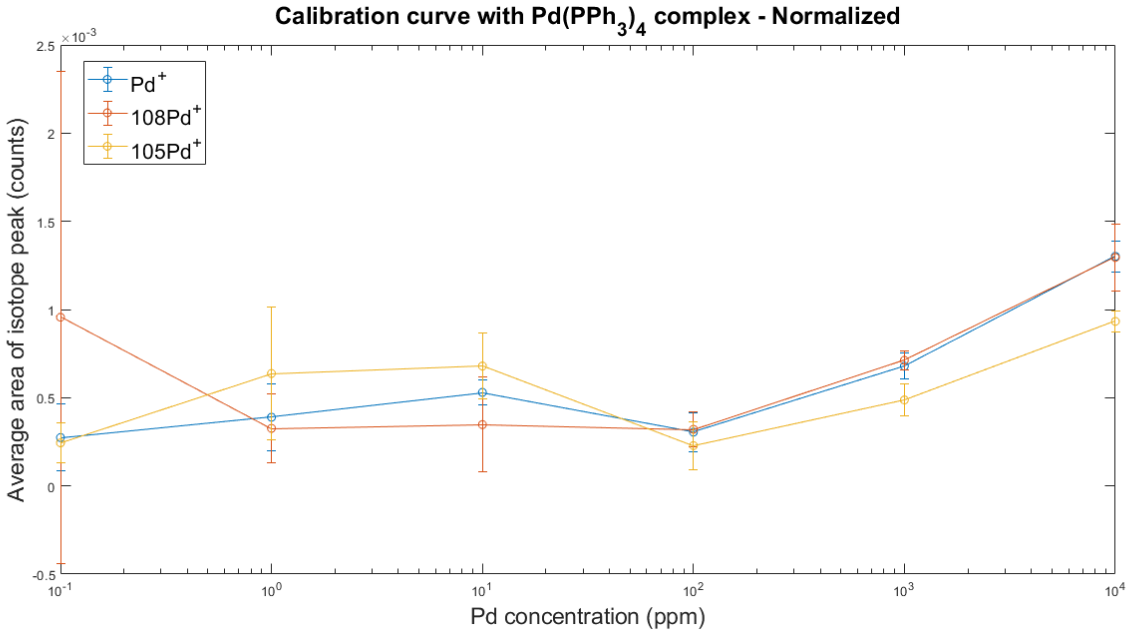

Figure 4.2: Calibration curve created from polymer samples with 0, 1, 10 100, 1000, 10,000 ppm Pd from $Pd(PPh_3)_4$. The average peak area and concentration of each sample normalized to total ion intensity count are plotted on the y-axis and x-axis, respectively. Standard deviation can be observed in the bars for each Pd point

The calibration curves in Figure 4.1 and 4.2 did not perform as expected regarding the linear fit. This could likely be due to sample preparation which should be improved. The $Pd(PPh_3)_4$ complex showed stability and solubility issues as incomplete dissolution in solution and degradation was observed, most likely caused by oxidation of the Pd complex. This could lead to not having the correct amount of Pd in the sample. In addition, the thin films were prepared by spin-coating the solution which poses contamination risks. The final coating consisted of a very thin film that appeared slightly uneven which can give discrepancies in the amount of data points obtained when depth profiling.

4.1.2 Calibration curve using $Pd_2(dba)_3 \cdot CHCl_3$ complex

To address the previous issues with the samples measured for the calibration curves in Figure 4.1 and 4.2, a more stable and soluble Pd complex was used. For the new calibration curve, a $Pd_2(dba)_3 \cdot CHCl_3$ complex which stabilizes and enhances the solubility in solution was used. For the samples prepared with $Pd_2(dba)_3$ complex, extra care was taken to reduce cross-contamination during preparation through extensive cleaning of the area and equipment used. To combat the previous issues with uneven thin films which could have led to discrepancies in the amount of data points obtained, thicker films were created through drop-casting. The solution was dropped onto thin films which was successful, however, aggregation on the surface was seen especially for the 10,000 ppm sample. Sputtering of the samples was done using argon as a source. A calibration curve was created from the values of the

TOF-SIMS measurement which is shown in Figure 4.3 and the values are not subjected to any normalization. For this measurement, the total ion count was similar between each isotope which led to smaller differences observed between normalizing to total ion count or nonnormalized. This likely means fewer variations in the experimental conditions such as different ionization efficiency. The standard deviation has decreased significantly compared to the graph in Figures 4.1 and 4.2. Films prepared with neat P3HT have a low Pd content likely due to the high care taken to avoid any possible Pd contamination sources. The Pd content is seen to slightly linearly increase following the increase in prepared Pd content from 1 to 100 ppm. This is followed by a larger increase to 1000 ppm and a major increase to 10,000 ppm. Using drop-casting and the $Pd_2(dba)_3 \cdot CHCl_3$ complex proved to be more successful most likely due to less contamination from spin-coating, thicker films and a higher soluble and stable complex which allowed for homogeneous solutions used.

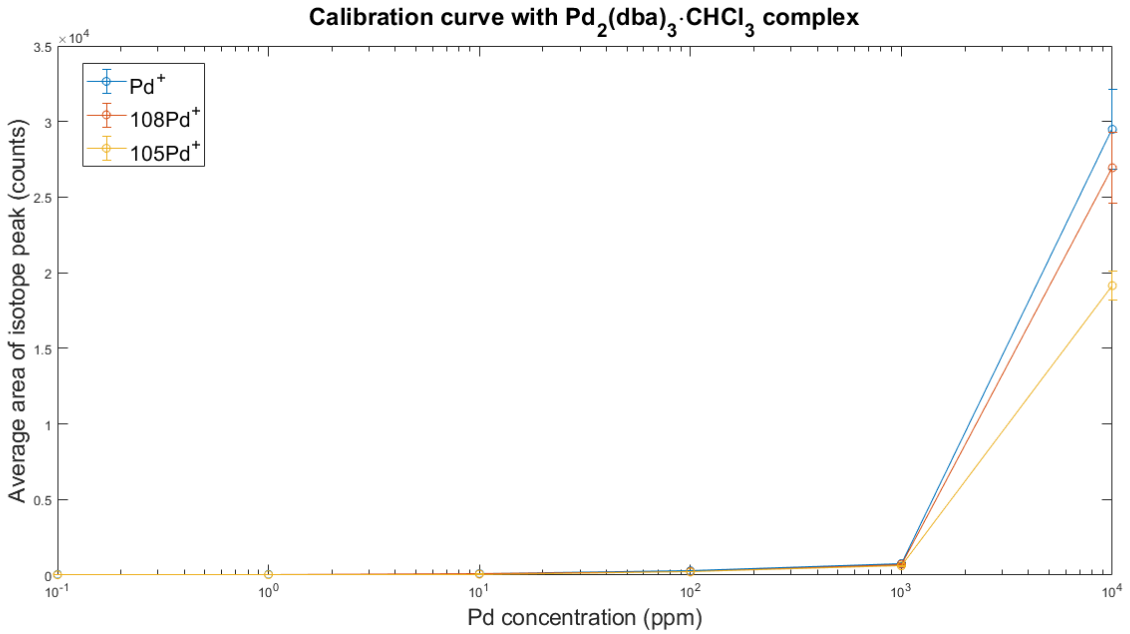

Figure 4.3: Calibration curve created from polymer samples with 0, 1, 10 100, 1000, 10,000 ppm Pd from $Pd_2(dba)_3 \cdot CHCl_3$ complex. The average peak area and concentration of each sample are plotted on the y-axis and x-axis, respectively. Standard deviation can be observed in the bars for each Pd point.

The large deviation of the average peak area for the 10,000 sample from the values measured in the range 0-1000 ppm in Figure 4.3, could likely be due to the high aggregation observed in the thin films for this sample. Due to the high concentration, it formed an uneven coating, hence measurement is likely impacted by the aggregation. Due to this deviation, the range of Pd concentration was modified to 0-1000 ppm, to account for the limitation in sample preparation at higher Pd content which is plotted in Figure 4.4. The average peak area measured can be seen to increase for Pd^+ and the two isotopes $105Pd^+$ and $108Pd^+$ from 0 to 1000 ppm, however, the curve does not possess complete linearity. Although complete linearity is not achieved, a clear trend can be seen between Pd samples with increased concentration

and the increase in the average peak area measured for each sample. For samples with a Pd concentration over 100 ppm, no overlap in standard deviation is observed which indicates that the values are significantly different, however, the overall trend proves the possibility of using TOF-SIMS to measure polymer samples. A regression model can be built from the linear fit which is utilized to calculate the Pd content from a polymer sample's measured average peak area signals.

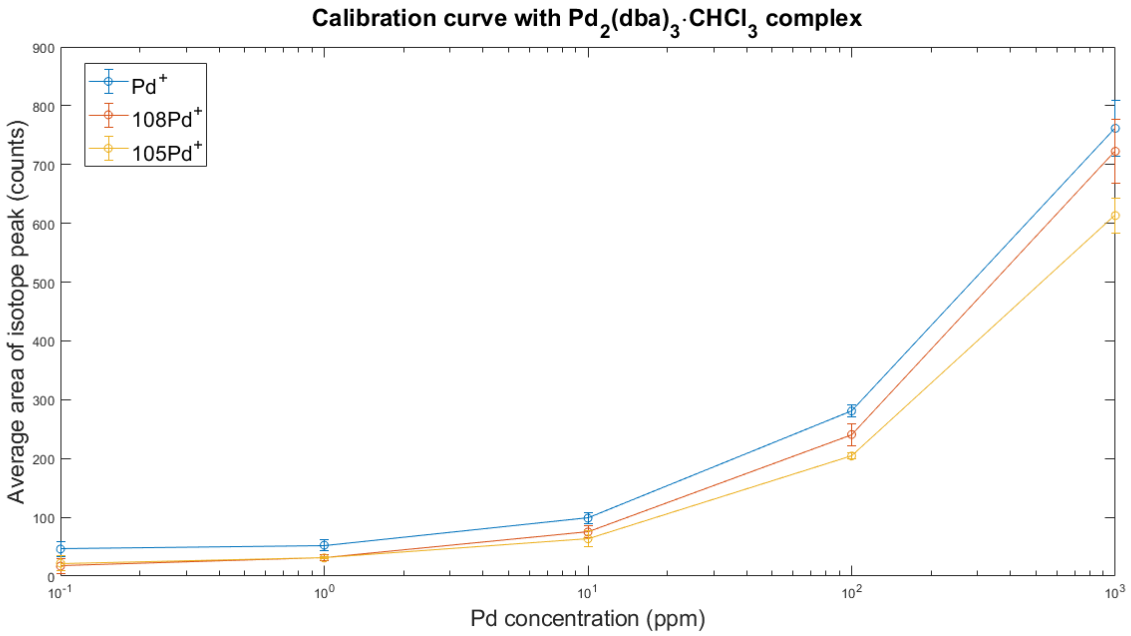

Figure 4.4: Calibration curve created from polymer samples with 0, 1, 10 100, 1000 ppm Pd from $Pd_2(dba)_3 \cdot CHCl_3$ complex. The average peak area and concentration of each sample are plotted on the y-axis and x-axis, respectively. Standard deviation can be observed in the bars for each Pd point.

4.2 Purificiation of D18

4.2.1 Soxhlet extraction of D18

From the Soxhlet extraction, insignificant amounts of D18 mass were collected from the fractions that had been extracted with acetone and hexane. However, an almost 100 % recovery of the neat D18 used was obtained in which 35 and 63 % yield of D18 were collected from the fractions extracted with $CHCl_3$ and THF, respectively.

The M_n, M_w, and Đ that were measured with GPC are shown in Table 4.1 for the two D18 fractions resulting from Soxhlet extraction with THF and $CHCl_3$. Unpurified D18 is also shown as a reference. It shows that THF removed smaller M_W and the $CHCl_3$ fraction shows a higher M_W and a narrower Đ than the THF fraction. The values of the THF and $CHCl_3$ fraction are high compared to neat D18 which might be a result of aggregation in the analytical GPC column.

Table 4.1: The M_n, M_w and Đ measured with GPC for fractions from Soxhlet extraction with the solvents THF and $CHCl_3$, respectively.

Sample	M_n (KDa)	M_w (KDa)	Đ
D18 neat	32	93	3
D18 THF Soxhlet fraction	38	287	7,6
D18 $CHCl_3$ Soxhlet fraction	201	820	4,1

In Figure 4.5 the chromatogram of the GPC analysis is shown for further clarification, along with neat D18 as a reference. Neat D18 can be observed to have the broadest peak which suggests a high Đ and its main peak indicates the presence of high M_W D18. Furthermore, the tail at the end indicates that it also contains lower M_W D18 fractions as well. D18 that was extracted with $CHCl_3$ shows a sharp peak at around 17 minutes which suggests a relatively higher M_W compared to neat D18 and the THF fraction. The sharp peak also indicates a lower Đ meaning that this sample is more uniform in M_W. D18 that was extracted with THF shows a slightly broader peak with some tailing at the end, indicating that this sample is more a mixture of high and low M_W with a higher Đ. The peak of THF is slightly more narrow than that of neat D18 which suggests that it purified it to some extent, removing some M_W compounds of D18. Comparing neat D18 and the $CHCl_3$ fraction it suggests effective purification with $CHCl_3$ with a smaller range of high M_W. However, the Đ is measured to be higher for the $CHCl_3$ fraction which could be due to the tailing of the neat D18 causing issues with the peak integration. To resolve this issue an alternative detector could be used such as a UV detector with a wavelength of 550 nm.

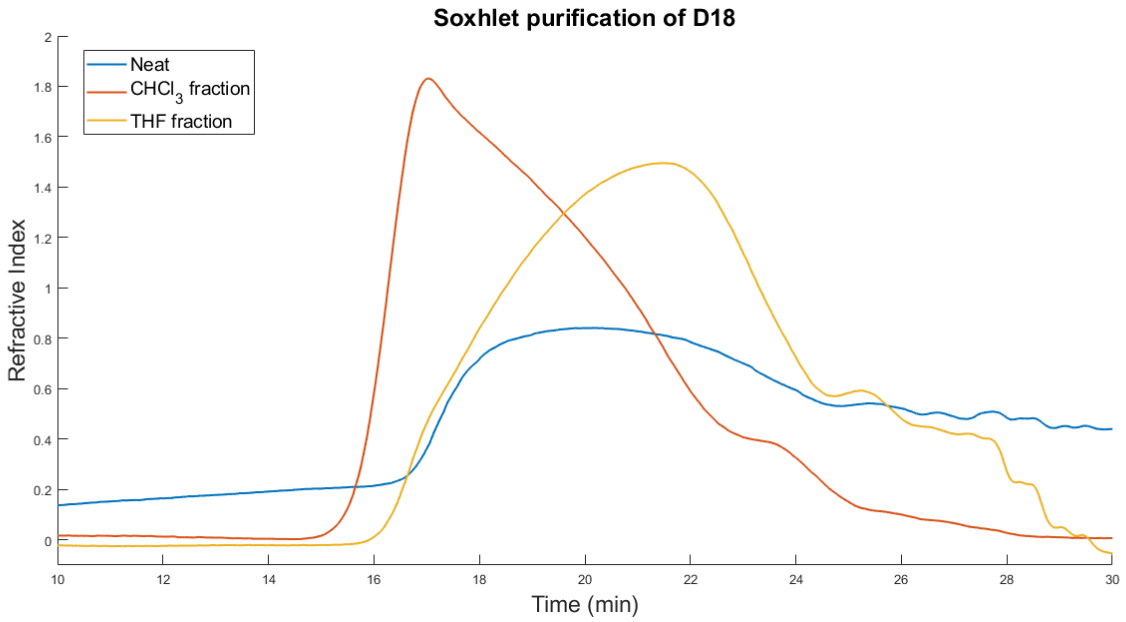

Figure 4.5: Chromatogram of GPC analysis for fractions from Soxhlet extraction with the solvents THF and $CHCl_3$, respectively.

4.2.2 HPLC purification of D18

The resulting UV-vis spectra from the purification of D18 using manual HPLC are shown in Figure 4.6. It can be seen that D18 absorbs strongly at 550 nm which are the 3 largest peaks. The collected D18 fractions are displayed as the pink, turquoise, yellow, and blue-shaded regions of 550 nm peaks. Furthermore, D18 appears to consist of a large fraction of low M_W observing the long tail of the two first peaks. The green-colored peaks show the recycled portion that is carried out to increase the effective column length which gives better separation of the polymer. As the first recycle broadened the second peak it is possible to separate the low M_W fractions of D18 so it does not mix with the higher M_W fraction. By separating low M_W fractions, narrower and higher M_W of D18 can be obtained. The major fraction collected was therefore the low M_W fraction 2 which typically would be discarded from the column to remove low M_Ws and is seen as the pink area. A higher M_W fraction was subsequently collected and observed as the turquoise area, which was followed by the collection of a medium and low M_W 1 fraction seen as the yellow and blue area, respectively.

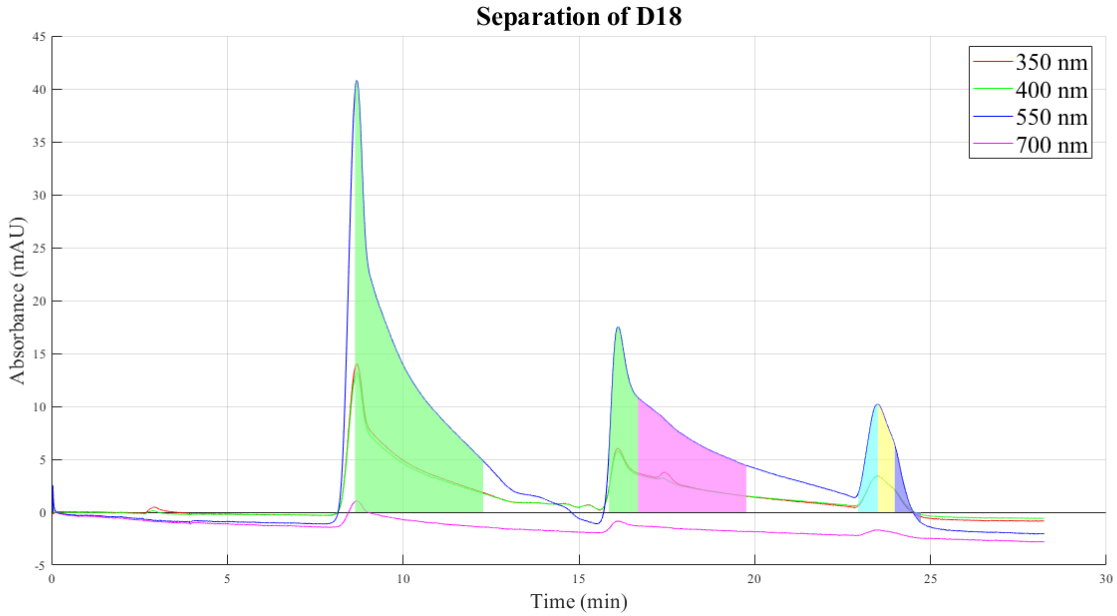

Figure 4.6: UV-vis spectra from the purification of D18 illustrating the absorbance of compounds detected at 350, 400, 550, and 700 nm and the time of the manual separation.

The polymer mass obtained from each fraction of D18 after HPLC purification is shown in Table 4.2. It can be seen that a very low total yield was obtained which shows a significant loss of polymer mass.

Table 4.2: Polymer mass collected from each D18 fraction purified with HPLC.

Fraction	Polymer mass (mg)	Yield (%)
D18 high M_W HPLC fraction	0.3	0.375
D18 medium M_W HPLC fraction	0.4	0.5
D18 low M_W HPLC fraction 1	0.3	0.375
D18 low M_W HPLC fraction 2	2.6	3.25

The M_n, M_w, and Đ that were measured with GPC are shown in Table 4.3 and it can be confirmed that a higher, medium, and low M_W was collected. The Đ is also shown to decrease compared to the neat polymer. The collection of the pink area in Figure 4.6, the low M_W fraction 2, has the lowest M_W and highest Đ of all HPLC fractions indicating that the purification was effective in removing smaller M_W D18. Similar to Table 4.1, the M_W values are high compared to neat D18 which can be a result of aggregation in the analytical GPC column.

Table 4.3: The M_n, M_w and Đ measured with GPC for fractions from the collected fractions of HPLC purification.

Sample	M_n (KDa)	M_w (KDa)	Đ
D18 neat	32	93	3
D18 high M_w HPLC fraction	859	1221	1.4
D18 medium M_w HPLC fraction	741	1018	1.4
D18 low M_w HPLC fraction 1	652	791	1.2
D18 low M_w HPLC fraction 2	286	462	1.6

In Figure 4.7 the chromatogram of the GPC analysis is shown for further clarification, along with neat D18 as a reference. As in Figure 4.5, the peak of neat D18 indicates a high Đ with a range of different M_W. The peak of the high M_w fraction is sharp and indicates that it has lower Đ than neat D18 and contains higher M_W as the compounds elute faster. Following this is the medium M_W fraction which shows a slightly broader peak than high M_W and a longer elution time which suggests a mixture of a range of different medium M_W compounds. The low M_W fraction 1 has a peak that is relatively narrow suggesting a lower Đ than the high and medium M_W fractions. Its elution time indicates that it also contains lower M_W compounds. The low M_W fraction 2 which was the first fraction collected from the HPLC purification shows the broadest peak of all fractions with a significant spread in retention times. The broad peak and latest elution time suggest that it contains the lowest M_W compounds with a high Đ. The chromatogram indicates that HPLC effectively separates the D18 sample into distinct fractions with different M_W and narrower Đ.

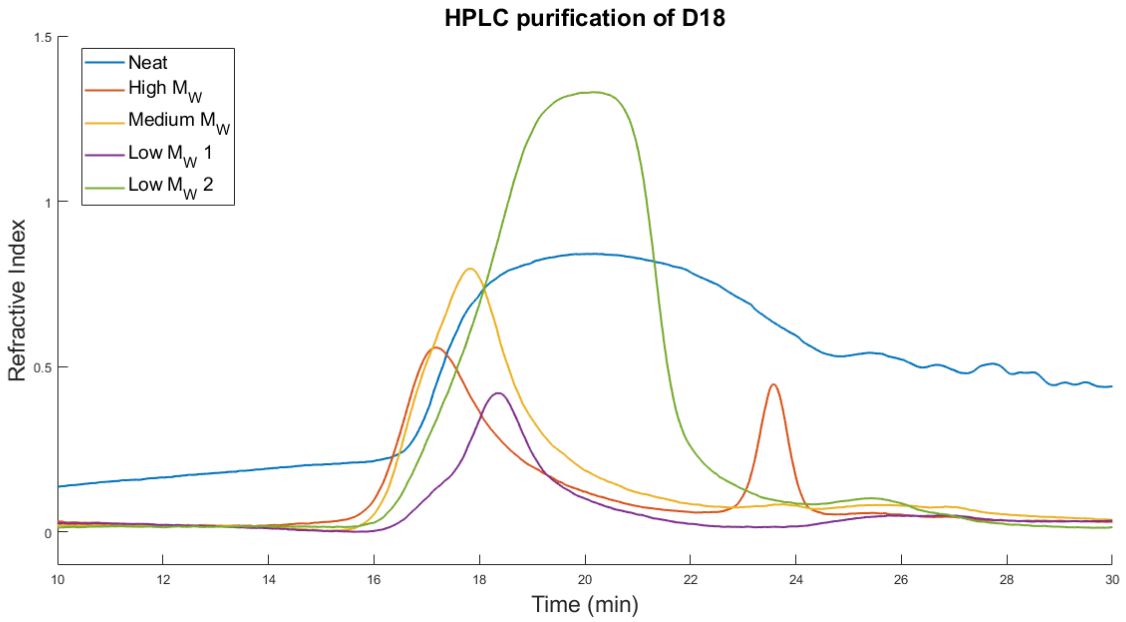

Figure 4.7: Chromatogram of GPC analysis for fractions from HPLC purification.

4.3 TOF-SIMS data analysis of polymer D18

4.3.1 Nonnormalized data measurement

After developing the method for Pd content evaluation using TOF-SIMS, the calibration curve developed in Figure 4.4 was used to investigate the efficiency of the various purification techniques used for the D18 polymer. Thin films of D18 samples, purified via HPLC and Soxhlet, were prepared and measured using TOF-SIMS.

As carried out for the calibration curve samples, the D18 samples were subject to TOF-SIMS analysis using in-depth profiling using an argon ion source. The calibration curve in Figure 4.4 and measured average peak areas for each sample were not subjected to any normalization. Through the measured average peak areas for each sample, the concentration of Pd content in ppm was calculated for each D18 sample using the regression model created from the calibration curve. This can be seen in Figure 4.8 and Table 4.4. On the y-axis in Figure 4.8, the calculated Pd content is shown and the standard deviation of each measurement of D18 samples with TOF-SIMS is observed in the bars. In Table 4.4 the average value of Pd content from each purification procedure of D18 is shown.

Figure 4.8 and Table 4.4 show unexpected increases in Pd content after both Soxhlet extraction and HPLC purification. A strong deviation from this, however, is the low content of Pd after Soxhlet extraction with THF as solvent. The samples, low M_W 2 and high M_W from HPLC and the acetone sample from Soxhlet extraction, also showed a decrease in Pd content. However, the notable decrease from the THF sample might indicate that using THF in Soxhlet extraction is efficient at removing Pd from D18. However, since the overall trend with an increase in Pd

content, prominently after HPLC purification is highly contradicting previous work, it indicates that the results are inconclusive[8][25][4]. Only above 100 ppm in the calibration curve in Figure 4.4, there is a significant difference in the area peak area measured. This indicates that all measured values below 100 ppm are not reliable. This might be a result of not normalizing the data which leads to variations in experimental conditions affecting the average peak area values.

In Figure 4.8 it can be seen that Pd^+ shows higher standard deviations for a majority of the D18 samples and the least difference in values is observed for the $105Pd^+$ and $108Pd^+$ isotopes. The content of Pd^+ is also observed to be higher for the samples which is likely due to its average peak area values reflecting the overall Pd signals representing all isotopes. This is therefore seen as a higher concentration of measured Pd. The higher standard deviation for Pd^+ might indicate that normalization is necessary and the measurement of Pd content differed largely due to different ionization efficiency.

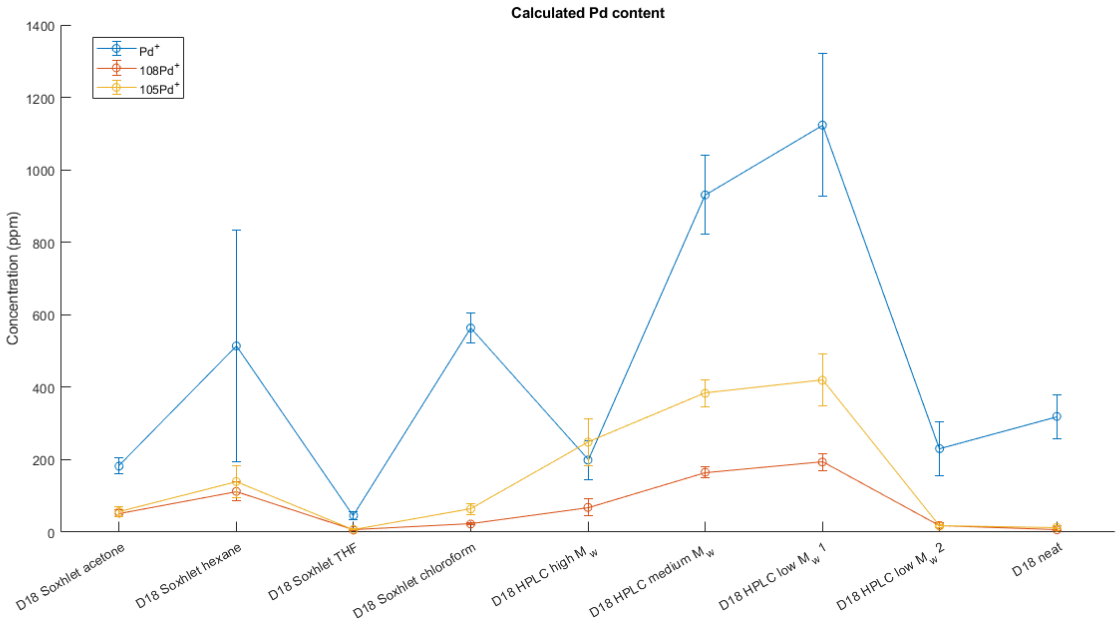

Figure 4.8: Pd content from in-depth profiling of neat D18 and D18 samples collected from HPLC purification and Soxhlet extraction calculated from the regression model. The measurement of D18 samples is nonnormalized and standard deviation is seen as the bars for each sample point.

The calculated average Pd content in ppm is shown in Table 4.4. The content of Pd^+ is seen to decrease for the acetone and THF fractions from Soxhlet extraction, with a drastic decrease for THF. It has also decreased in the HPLC fractions from low M_W 2 and high M_W. $105Pd^+$ and $108Pd^+$is are observed to have a major increase in Pd content for all D18 samples compared to neat D18 except for the D18 sample collected after Soxhlet extraction using THF. As noted in Figure 4.8, the results point to the necessity of normalizing the values.

Table 4.4: The average amount of Pd^+, $108Pd^+$, and $105Pd^+$ in ppm calculated for each D18 sample from the in-depth profiling with TOF-SIMS and nonnormalized.

Sample	Pd^+ content (ppm)	$108Pd^+$ content (ppm)	$105Pd^+$ content (ppm)
D18 acetone Soxhlet fraction	182.27	52.36	56.693
D18 hexane Soxhlet fraction	514.07	112.48	139.54
D18 THF Soxhlet fraction	46.027	5.67	7.67
D18 $CHCl_3$ fraction	536.46	22.34	64.04
D18 high M_W HPLC fraction	199	68.4	248.18
D18 medium M_W HPLC fraction	930.79	165.33	383.19
D18 low M_W HPLC fraction 1	1123.4	193.41	419.13
D18 low M_W HPLC fraction 2	230.42	18.67	16.67
D18 neat	319.4	6.33	13.33

4.3.2 Normalized data measurement

To improve the previously encountered issues with nonnormalized data, the average peak area values from each D18 sample after Soxhlet extraction and HPLC purification were normalized to various signals. This included normalizing both the calibration curve and the D18 samples to the same signal. Normalization of the calibration curve and D18 samples to total ion count resulted in unreasonable low values regarding the Pd concentration of the samples. The calibration curve normalized total ion count was, however, very similar to the nonnormalized calibration curve in Figure 4.4. In contrast, normalization to the total ion count of the average peak areas of the D18 samples did not impact the values, as previously observed for the measurements in section 4.1.1. The reason might be that the total ion count includes the contribution from all ions, regardless of ionization efficiency which can skew the normalization. Differences between the samples such as the homogeneity and contaminants could likely be a cause for this, hence the D18 sample values did not respond as well as the calibration curve to this normalization.

Normalizing to a polymer fragment of D18 that ionizes consistently can likely improve the results, accounting for matrix effects, and reducing the effect of contaminations. Argon which was used as a source in the TOF-SIMS measurement is good at ionizing samples with organic compounds. The measured Pd average peak areas are small in comparison to organic compounds, hence normalizing to an organic fragment could help eliminate the influence of inorganic contaminants. It was found that the alkane fragment C_4H_{10} showed suiting values regarding ionization efficiency, hence both the calibration curve and the D18 sample's average peak area values were normalized to C_4H_{10}. The resulting calibration curve is shown in Figure 4.9. It can be seen that the standard deviation has increased for the 100 and 1000 ppm points compared to the calibration curve in Figure 4.4 with some overlapping average peak area counts. This indicates that the values of the 100 and 1000 ppm points are not significantly different which can lead to less reliable estimations of Pd content. Below 100 ppm, the standard deviation is lower and similar to those seen in Figure 4.4. Compared to the calibration curve in Figure 4.4, this calibration curve normalized

to an alkane fragment could, therefore, for the 100 and 1000 ppm points give less reliable Pd estimations. A completely linear fit of the regression model is still not achieved with normalization to an alkane fragment. However, a general increase in concentration is seen which was also observed in Figure 4.4.

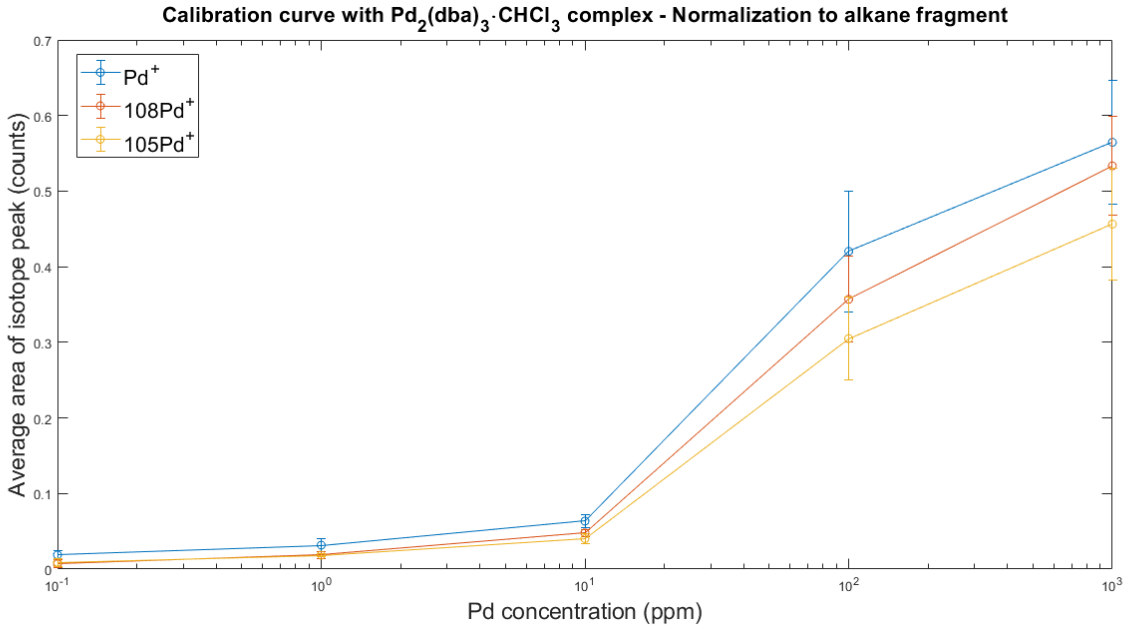

Figure 4.9: Calibration curve normalized to an alkane fragment created from polymer samples with 0, 1, 10 100, 1000 ppm Pd from $Pd_2(dba)_3 \cdot CHCl_3$ complex. The average peak area and concentration of each sample are plotted on the y-axis and x-axis, respectively. Standard deviation can be observed in the bars for each Pd point.

Through the normalized measured average peak areas for each sample, the concentration of Pd content in ppm was calculated for each D18 sample using the regression model created from the calibration curve in Figure 4.9. This can be seen in Figure 4.10 and Table 4.5. On the y-axis in Figure 4.10, the calculated Pd content is shown and the standard deviation of each measurement of D18 samples with TOF-SIMS is observed in the bars. In Table 4.5 the average value of Pd content from each purification procedure of D18 is shown.

Figure 4.10 and Table 4.5 show significantly different trends compared to the trends seen in Figure 4.8 and Table 4.4. The overall Pd content has decreased after both Soxhlet extraction and HPLC purification. This is in accordance with previous studies in which both purification methods can reduce Pd content to varying degrees[8][25][4]. From the acetone and hexane fraction of Soxhlet extraction, the least Pd content is observed, however, this is likely due to the negligible amount of D18 extracted. Since Pd binds strongly to the polymer it does not indicate that these solvents were effective in reducing Pd content. In contrast, the solvent THF that extracted more than half of the original D18 mass showed a large decrease in Pd content. This can be explained by the D18 containing a high portion of low M_W.

The $CHCl_3$ fraction contains the higher M_W fraction of D18 and shows a similar amount of Pd as the neat D18 sample which might indicate that Pd binds strongly to higher M_W of D18.

For HPLC purification the high M_W fraction of D18 showed a large reduction in Pd content suggesting that HPLC can successfully remove Pd to an extent. The slower eluting fractions medium M_W and low M_W had similar Pd content which was lower than for high M_W, suggesting that slower eluting fractions are more purified. In addition, the second low M_W fraction was the first fraction collected and had the highest Pd content while it contained a large part of the low M_W D18. Together, this points to HPLC being effective at removing Pd content.

In Figure 4.10 it can be seen that overall the standard deviation is low, and more prominent for the two isotopes $105Pd^+$ and $108Pd^+$. This is likely due to a more consistent ionization efficiency of the isotopes. The overall Pd content which is reflected in Pd^+ shows a major increase in concentration, likely due to its aggregated values of isotopes. Hence, the overall higher standard deviations can be a cause of the different ionization energies of isotopes.

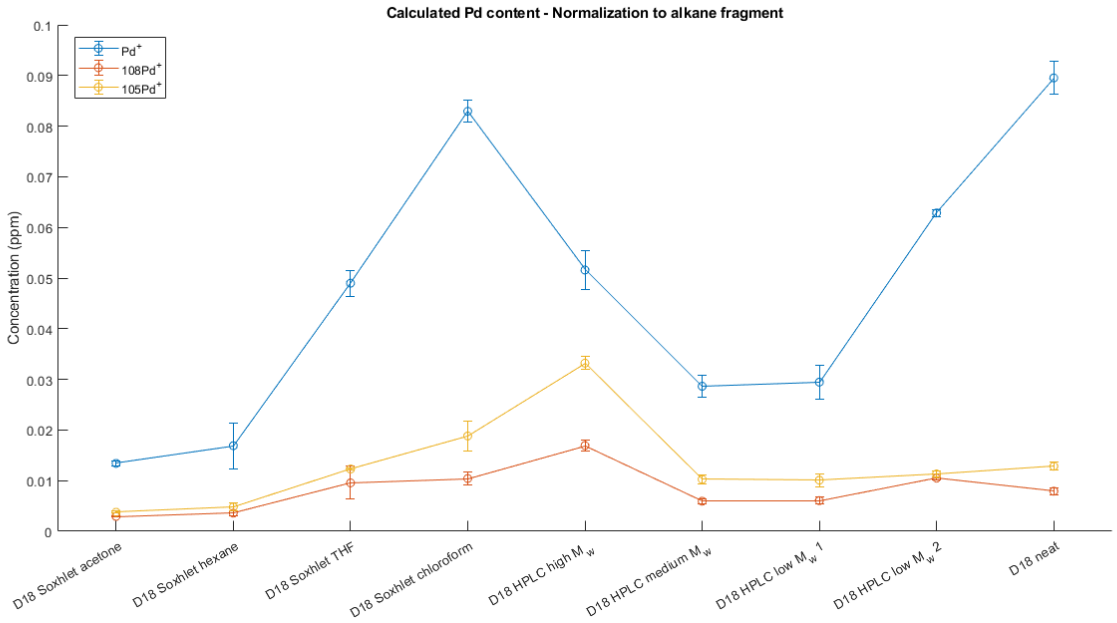

Figure 4.10: Pd content from in-depth profiling of neat D18 and D18 samples collected from HPLC purification and Soxhlet extraction calculated from the regression model. The measurement of D18 samples is normalized to an alkane fragment and the standard deviation is seen as the bars for each sample point.

The calculated average Pd content in ppm is shown in Table 4.5. It is seen that for the two isotopes $105Pd^+$ and $108Pd^+$, the Pd content increases somewhat in the D18 fraction from Soxhlet extraction using $CHCl_3$ and the higher M_W from HPLC purification. The THF fraction from Soxhlet extraction also increases slightly for $108Pd^+$. This can be attributed to the slight difference in ionization energy of isotopes but generally, the isotopes follow the same pattern as the general Pd content. In all

purified samples from both Soxhlet extraction and HPLC purification, the overall Pd content decreased which indicates that the normalization to an alkane fragment improved the results. However, the ppm values are significantly low compared to other studies utilizing Inductively coupled plasma mass spectrometry (ICP-MS) and show that there are still some issues to be resolved around normalization and how it impacts the fitted model predictions[8][25].

Table 4.5: The amount of Pd^+, $108Pd^+$ and $105Pd^+$ in ppm calculated for each D18 sample from the in-depth profiling with TOF-SIMS and normalized to alkane fragment.

Sample	Pd^+ content (10^{-3} ppm)	$108Pd^+$ content (10^{-3} ppm)	$105Pd^+$ content (10^{-3} ppm)
D18 acetone Soxhlet fraction	13.4	2.9	3.8
D18 hexane Soxhlet fraction	16.9	3.6	4.8
D18 THF Soxhlet fraction	48.9	9.5	12.3
D18 $CHCl_3$ fraction	82.9	10.4	18.8
D18 high M_W HPLC fraction	51.6	16.9	33.2
D18 medium M_W HPLC fraction	28.6	5.9	10.2
D18 low M_W HPLC fraction 1	29.4	6.1	10.1
D18 low M_W HPLC fraction 2	62.8	10.5	11.3
D18 neat	89.5	7.9	12.8

5

Discussion

From the results, it is apparent that the choice of the Pd complex has a significant impact on the possibility of creating a calibration curve. The Pd was added for both only through blending which means that a more soluble Pd complex is beneficial. The preparation of samples also differed between the two curves which is another factor that potentially positively influenced the results. For the first calibration curve using a $Pd(PPh_3)_4$ complex, solubility and stability issues were observed as the complex did not fully dissolve and oxidized easily. The polymer solution was then spin-coated on thin films which posed contamination risks and resulted in a thin and slightly uneven coating. For the second calibration curve using a $Pd_2(dba)_3 \cdot CHCl_3$ complex, the previous issues seen were resolved as this complex dissolved in solution and has a higher stability. To address the contamination and coating issues, samples were prepared by drop-casting in a thoroughly clean area. The resulting coating was more homogeneous and thicker which suited well for in-depth profiling with TOF-SIMS.

The initial calibration curve created using P3HT and the $Pd(PPh_3)_4$ complex seemed to work better for higher Pd concentration compared to the second calibration curve using a $Pd_2(dba)_3 \cdot CHCl_3$ complex. However, large standard deviations were observed, and the isotopes showed inconsistent patterns regarding the amount of content. To improve the results, the data was normalized to total ion intensity count and this provided a better linear fit that accounted for variations in experimental conditions such as ionization efficiency. The standard deviations for Pd^+ were smaller, however, the average peak area measured is not seen to be significantly different for each concentration sample. This means that the calibration curve would give less reliable estimations of Pd content. Furthermore, major standard deviations and overlapping average peak areas measured were observed for the two Pd isotopes. Large variations in measured Pd content relative to the known concentration particularly at 100 ppm were also seen, indicating that the results were inconclusive.

Changing the complex to the $Pd_2(dba)_3 \cdot CHCl_3$ complex and the preparation method to create thicker sample films proved beneficial for the lower concentrations. Using a more soluble complex increases the chance of each sample being representative of its concentration due to improved homogeneity of the films. The standard deviations also decreased significantly for all isotopes which suggests more reliable and reproducible results. However, the 10,000 ppm data point deviated significantly, likely caused by large Pd aggregates, and was therefore removed from the analysis. For this calibration curve using the $Pd_2(dba)_3 \cdot CHCl_3$ complex, however, an

increase can be observed in both the general Pd content and the concentrations of $105Pd^+$ and $108Pd^+$. Despite the improvements, the curve did not exhibit complete linearity, and the presence of Pd at 0 ppm persisted.

The presence of Pd at 0 ppm continued to remain an issue throughout sample preparation which might indicate the need for even more strict protocols or cleaner environments. While the use of a more stable and soluble complex improved the calibration curve, achieving complete linearity and eliminating contamination remains a goal. The contribution from atmospheric and environmental contamination can be a difficult issue to resolve, however, requiring the use of a cleanroom which would affect the accessibility of measuring polymer samples with TOF-SIMS. Future work should therefore focus on improving sample preparation methods and testing additional normalization techniques to enhance the reliability and accuracy of calibration curves in TOF-SIMS analysis.

The regression model derived from the calibration curve using a $Pd_2(dba)_3 \cdot CHCl_3$ complex was expected to provide a linear fit that allowed the calculation of Pd concentrations from the measured average peak areas. However, both the model and normalization were observed to be critical for the results. When using the curve to analyze the Pd content in purified D18 samples, the first set of calculations without normalization showed an unexpected increase in Pd content after purification. This increase was seen in most samples, except for the D18 sample subjected to Soxhlet extraction with THF, which showed a significant decrease in Pd content. More samples also showed a decrease however the THF fraction was most notable and might suggest that THF is efficient at removing Pd from D18. However, since the trend seen here is highly contradicting previous work, it indicates that the results are inconclusive.

Normalization to the total ion count of the calibration curve and D18 samples gave a calibration curve similar to the nonnormalized curve. However, it did not improve the results for the calculation of Pd concentration in the D18 samples since the values were unreasonably low. Normalization to total ion count might not work as well for the D18 values since the total ion count includes the contribution from all ions, regardless of ionization efficiency which can skew the normalization. Differences between the samples such as the homogeneity and contaminants could be a cause for this.

When the calibration curve and D18 samples were normalized to an ion alkane fragment, higher values of Pd concentration were obtained, however, they were still observed to be low compared to literature[8][25]. Normalizing to a polymer fragment of D18 that ionizes consistently might account for matrix effects, and reduce the effect of contaminations. The alkane fragment C_4H_{10} showed consistent ionization and was therefore used for normalization. The resulting calibration curve showed less linearity and more overlapping average peak areas measured for the 100 and 1000 ppm points compared to the nonnormalized curve. However, the overall Pd content, excluding the isotopes $105Pd^+$ and $108Pd^+$, that was calculated from this calibration curve showed a decrease after all purification methods, which aligns with previous studies indicating that purification methods, Soxhlet extraction, and HPLC, can effectively reduce Pd content to varying degrees[8][25][4]. For HPLC,

the first eluting fractions contained the most Pd, which suggests that slower eluting fractions are more purified from Pd. There is a notable difference between the higher and medium fractions collected which were eluting closely and might indicate that Pd has a higher tendency to remain in the polymer matrix of high M_W. The two low fractions from HPLC are significantly different in Pd content, the one collected first contained the lowest M_W but the highest Pd content. The other low fraction was collected last in the HPLC procedure and showed a large decrease in Pd content, also indicating that slower eluting fractions are more purified.

For the Soxhlet extraction, the fraction of THF consisted of more than half of the original D18 mass and showed a significant Pd content decrease. This might be attributed to the high dissolution of lower M_W D18 in THF which in turn might reduce Pd binding. This is especially seen in the $CHCl_3$ fraction that likely consists of a smaller range of high M_W. It almost contains the same amount of Pd as the neat D18 sample, similar to the results from HPLC that indicate that Pd might bind stronger to higher M_W. The acetone and hexane fraction showed very low Pd content and likely contained different contaminants and lower M_W parts.

However, the Pd content values from the calculations of normalization to an alkane fragment are still low compared with values in literature, based on the absolute ICP-MS method, and show the need for an optimized normalization of the data[8][25]. Several different normalization techniques were tested and they all showed similar trends in the relative concentration of D18 samples. However, the ppm values differed significantly with some showing unreasonable low values. It confirms that normalization gives more reliable results, however, only a trend can be reported and not an absolute quantification. The differences between the initial and normalized results highlight the sensitivity of the fitted model to normalization. The normalization process in turn impacts the predicted ppm values which indicates potential issues with the initial model calibration or the need for more robust normalization techniques to ensure accurate predictions and quantification.

After purification of D18 with HPLC, a yield of less than 5% was obtained. It showed a major loss of polymer mass and shows the need for complete dissolution since D18 tends to aggregate. Hence, loss of mass can have occurred in multiple steps such as in preparation when filtering the solution. It might also have aggregated and stuck to the column in HPLC. It shows the importance of finding a protocol for the complete dissolution of D18 to enable further experiments and to obtain higher M_W. It was also observed in the UV-vis spectra from HPLC and GPC data that it contained a large fraction of low M_W. A large portion of the mass lost is likely the low M_W fractions that were sent to waste. This can also explain why THF in Soxhlet extraction could dissolve a majority of the sample since the D18 sample consisted to a large extent of low M_W. It highlights the importance of purification to obtain a high M_W neat polymer sample with low Đ that will produce reliable results when used in electronic and optical applications.

The Soxhlet extraction was shown to be less effective than HPLC to narrow down the Đ of the D18. Although it was highly effective in removing low M_W, the HPLC could narrow down the distribution to a larger extent. Both purification methods showed trends of decreasing the Pd content however further work should focus on

improving the handling and dissolution of D18 to create better results and avoid any loss.

Bibliography

[1] Nerea Casado et al. “Current trends in redox polymers for Energy and Medicine”. In: *Progress in Polymer Science* 52 (Jan. 2016), pp. 107–135. DOI: 10.1016/j.progpolymsci.2015.08.003 (cit. on p. 1).

[2] James H. Bannock et al. “The influence of polymer purification on the efficiency of poly(3-hexylthiophene):fullerene organic solar cells”. In: *Scientific Reports* 6.1 (Mar. 2016). DOI: 10.1038/srep23651 (cit. on p. 1).

[3] Christopher Bracher et al. “The effect of residual palladium catalyst on the performance and stability of PCDTBT:PC70BM Organic Solar Cells”. In: *Organic Electronics* 27 (Dec. 2015), pp. 266–273. DOI: 10.1016/j.orgel.2015.10.001 (cit. on pp. 1, 4).

[4] Junpei Kuwabara et al. “Effects of the terminal structure, purity, and molecular weight of an amorphous conjugated polymer on its photovoltaic characteristics”. In: *ACS Applied Materials amp; Interfaces* 8.3 (Jan. 2016), pp. 1752–1758. DOI: 10.1021/acsami.5b09482 (cit. on pp. 1, 3, 5, 23, 25, 29).

[5] Niklas Björklund et al. “The effects of metal impurities in poly[(2,5-bis(3-decylthiophen-2-yl)thieno(2,3-b]thiophene) on field-effect transistor properties”. In: *Organic Electronics* 10 (2 2009). ISSN: 15661199. DOI: 10.1016/j.orgel.2008.11.005 (cit. on p. 1).

[6] Jeonghun Kim, Jung Ho Kim, and Katsuhiko Ariga. “Redox-active polymers for Energy Storage Nanoarchitectonics”. In: *Joule* 1.4 (Dec. 2017), pp. 739–768. DOI: 10.1016/j.joule.2017.08.018 (cit. on p. 1).

[7] Philip Rohland et al. “Redox-active polymers: The magic key towards energy storage – A polymer design guideline progress in Polymer Science”. In: *Progress in Polymer Science* 125 (Feb. 2022), p. 101474. DOI: 10.1016/j.progpolymsci.2021.101474 (cit. on p. 1).

[8] Sophie Griggs et al. “The effect of residual palladium on the performance of organic electrochemical transistors”. In: *Nature Communications* 13.1 (Dec. 2022). DOI: 10.1038/s41467-022-35573-y (cit. on pp. 1, 5–7, 23, 25, 27, 29, 30).

[9] Mathieu Urien et al. “Field-effect transistors based on poly(3-hexylthiophene): Effect of impurities”. In: *Organic Electronics* 8.6 (Dec. 2007), pp. 727–734. DOI: 10.1016/j.orgel.2007.06.003 (cit. on p. 1).

[10] Feng Liu et al. “Molecular weight dependence of the morphology in P3HT:PCBM solar cells”. In: *ACS Applied Materials and Interfaces* 6 (22 2014). ISSN: 19448252. DOI: 10.1021/am505283k (cit. on pp. 1, 2, 4).

[11] Han Yan Wu et al. “Influence of Molecular Weight on the Organic Electrochemical Transistor Performance of Ladder-Type Conjugated Polymers”. In: *Advanced Materials* 34 (4 2022). ISSN: 15214095. DOI: 10.1002/adma.202106235 (cit. on pp. 1, 2, 4).

[12] Shotaro Hayashi, Shin Ichi Yamamoto, and Toshio Koizumi. “Effects of molecular weight on the optical and electrochemical properties of EDOT-based -conjugated polymers”. In: *Scientific Reports* 7 (1 2017). ISSN: 20452322. DOI: 10.1038/s41598-017-01132-5 (cit. on pp. 1, 2, 4).

[13] Rodrigo Noriega et al. “A general relationship between disorder, aggregation and charge transport in conjugated polymers”. In: *Nature Materials* 12 (11 Nov. 2013), pp. 1038–1044. ISSN: 14761122. DOI: 10.1038/nmat3722 (cit. on pp. 1, 4).

[14] Akhtar Hussain Malik et al. *A short review article on conjugated polymers*. Mar. 2023. DOI: 10.1007/s10965-023-03451-w (cit. on p. 3).

[15] Klaus Müllen and Ullrich Scherf. *Conjugated Polymers: Where We Come From, Where We Stand, and Where We Might Go*. Feb. 2023. DOI: 10.1002/macp.202200337 (cit. on p. 3).

[16] Zhitao Zhang et al. “Conjugated Polymers for Flexible Energy Harvesting and Storage”. In: *Advanced Materials* 30 (13 Mar. 2018). ISSN: 15214095. DOI: 10.1002/adma.201704261 (cit. on p. 3).

[17] Ahmed G.S. Al-Azzawi et al. *A Mini Review on the Development of Conjugated Polymers: Steps towards the Commercialization of Organic Solar Cells*. Jan. 2023. DOI: 10.3390/polym15010164 (cit. on p. 3).

[18] Xiaowei Zhong et al. “Facile Synthesis of Key Building Blocks of D18 Series Conjugated Polymers for High-Performance Polymer Solar Cells”. In: *ACS Applied Polymer Materials* 5 (3 Mar. 2023), pp. 1937–1944. ISSN: 26376105. DOI: 10.1021/acsapm.2c02009 (cit. on pp. 3, 4).

[19] Ke Jin, Zuo Xiao, and Liming Ding. “D18, an eximious solar polymer!” In: *Journal of Semiconductors* 42 (1 Jan. 2021). ISSN: 16744926. DOI: 10.1088/1674-4926/42/1/010502 (cit. on p. 3).

[20] Ossila. “D18”. In: () (cit. on pp. 3, 4).

[21] Dingding Qiu et al. *The Crystallinity Control of Polymer Donor Materials for High-Performance Organic Solar Cells*. Nov. 2020. DOI: 10.3389/fchem.2020.603134 (cit. on pp. 3, 4).

[22] Qishi Liu et al. “18% Efficiency organic solar cells”. In: *Science Bulletin* 65 (4 Feb. 2020), pp. 272–275. ISSN: 20959281. DOI: 10.1016/j.scib.2020.01.001 (cit. on pp. 3, 4).

[23] Zhiyong Liu and Hongen Wang. “Ternary polymer solar cells by employing two well-compatible donors with cascade energy levels”. In: *Dyes and Pigments* 192 (Aug. 2021). ISSN: 18733743. DOI: 10.1016/j.dyepig.2021.109424 (cit. on pp. 4, 11).

[24] Anping Zeng et al. “A Chlorinated Donor Polymer Achieving High-Performance Organic Solar Cells with a Wide Range of Polymer Molecular Weight”. In: *Advanced Functional Materials* 31 (33 Aug. 2021). ISSN: 16163028. DOI: 10.1002/adfm.202102413 (cit. on p. 4).

[25] Jan Kosco and Iain McCulloch. “Residual PD enables photocatalytic H2 evolution from conjugated polymers”. In: *ACS Energy Letters* 3.11 (Oct. 2018), pp. 2846–2850. DOI: 10.1021/acsenergylett.8b01853 (cit. on pp. 5, 7, 23, 25, 27, 29, 30).

[26] July 2022. URL: https://chembam.com/definitions/soxhlet-extractor/ (cit. on p. 5).

[27] Chi Kin Lo, Rylan M.W. Wolfe, and John R. Reynolds. “From monomer to conjugated polymer: A perspective on best practices for synthesis”. In: *Chemistry of Materials* 33 (13 July 2021), pp. 4842–4852. ISSN: 15205002. DOI: 10.1021/acs.chemmater.1c01142 (cit. on p. 5).

[28] Eni Generalic. *Soxhlet extractor*. June 2022 (cit. on p. 6).

[29] Daniela Held and Peter Kilz. “Size-exclusion chromatography as a useful tool for the assessment of polymer quality and determination of macromolecular properties”. In: *Chemistry Teacher International* 3.2 (June 2021), pp. 77–103. DOI: 10.1515/cti-2020-0024 (cit. on pp. 6, 7).

[30] Agilent Technologies Inc. “An Introduction to Gel Permeation Chromatography and Size Exclusion Chromatography”. In: *Primer* (2015) (cit. on p. 6).

[31] Ryan A Fair et al. *Molecular Weight Characterization of Conjugated Polymers through Gel Permeation Chromatography and Static Light Scattering* (cit. on p. 7).

[32] Whisnant David. “Polymer Chemistry: Molecular Weight Averages”. In: (cit. on p. 7).

[33] Feifei Jia, Xia Zhao, and Yao Zhao. *Advancements in ToF-SIMS imaging for life sciences*. 2023. DOI: 10.3389/fchem.2023.1237408 (cit. on pp. 7, 8).

[34] Teo Lombardo et al. “ToF-SIMS in battery research: Advantages, limitations, and best practices”. In: *Journal of Vacuum Science Technology A* 41 (5 Sept. 2023). ISSN: 0734-2101. DOI: 10.1116/6.0002850 (cit. on pp. 7, 8).

A

Appendix 1

Table A.1: Amounts of used $Pd(PPh_3)_4$ and chlorobenzene for serial dilution to create concentrations of 1, 10, 100, 1000, 10,000 ppm in polymer solution.

Vial 1	Vial 2	Vial 3	Vial 4	Vial 5
30 mg of $Pd(PPh_3)_4$	25 μl of vial 1	25 μl of vial 2	25 μl of vial 3	25 μl of vial 4
250 μl of chlorobenzene	225 μl of chlorobenzene	225 μl of chlorobenzene	225 μl of chlorobenzene	225 μl of chlorobenzene

Table A.2: Amounts of used $Pd_2(dba)_3 \cdot CHCl_3$ and chlorobenzene for serial dilution to create concentrations of 1, 10, 100, 1000, 10,000 ppm in polymer solution.

Vial 1	Vial 2	Vial 3	Vial 4	Vial 5
107,96093 mg of $Pd_2(dba)_3 \cdot CHCl_3$	200 μl of vial 1	200 μl of vial 2	200 μl of vial 3	200 μl of vial 4
2000 μl of chlorobenzene	1800 μl of chlorobenzene	1800 μl of chlorobenzene	1800 μl of chlorobenzene	1800 μl of chlorobenzene

DEPARTMENT OF SOME SUBJECT OR TECHNOLOGY
CHALMERS UNIVERSITY OF TECHNOLOGY
Gothenburg, Sweden
www.chalmers.se

CHALMERS
UNIVERSITY OF TECHNOLOGY